
01 Oct 2022

Hanford Low-activity Waste Glass Composition-temperature-melt Viscosity Relationships

Alejandro Heredia-Langner

Vivianaluxa Gervasio

Scott K. Cooley

Charmayne E. Lonergan

Missouri University of Science and Technology, clonergan@mst.edu

et. al. For a complete list of authors, see https://scholarsmine.mst.edu/matsci_eng_facwork/3215

Follow this and additional works at: https://scholarsmine.mst.edu/matsci_eng_facwork

 Part of the [Materials Science and Engineering Commons](#)

Recommended Citation




A. Heredia-Langner et al., "Hanford Low-activity Waste Glass Composition-temperature-melt Viscosity Relationships," *International Journal of Applied Glass Science*, vol. 13, no. 4, pp. 514 - 525, Wiley, Oct 2022.

The definitive version is available at <https://doi.org/10.1111/ijag.16580>

This Article - Journal is brought to you for free and open access by Scholars' Mine. It has been accepted for inclusion in Materials Science and Engineering Faculty Research & Creative Works by an authorized administrator of Scholars' Mine. This work is protected by U. S. Copyright Law. Unauthorized use including reproduction for redistribution requires the permission of the copyright holder. For more information, please contact scholarsmine@mst.edu.

RESEARCH ARTICLE

Hanford low-activity waste glass composition-temperature-melt viscosity relationships

Alejandro Heredia-Langner¹ | Vivianaluxa Gervasio¹ | Scott K. Cooley¹ | Charmayne E. Lonergan¹  | Dong-Sang Kim¹ | Albert A. Kruger²  | John D. Vienna¹ 

¹Pacific Northwest National Laboratory, Richland, Washington, USA

²US Department of Energy, Office of River Protection, Richland, Washington, USA

Correspondence

John Vienna, Pacific Northwest National Laboratory, Richland, WA 99352, USA.
Email: john.vienna@pnnl.gov

Funding information

U.S. Department of Energy (DOE) Office of River Protection (ORP); Waste Treatment Plant Project

Abstract

This study developed a model for predicting viscosity of alkali-alumino-borosilicate glass melts as functions of composition and temperature. The model is based on a total of 3935 viscosity-temperature data from 574 glasses with viscosity values ranging from 2.53 to 7260 Poise (P) in the temperature range of 900–1260°C. Several different model forms were surveyed, including those based on Arrhenius, Vogel-Fulcher-Tammann, Avramov-Milchev, and Mauro-Yue-Ellison-Gupta-Allen. For each of these models, combinations of the temperature-independent parameters were fitted to composition. It was found that generally fitting more than one temperature-independent parameter as functions of composition resulted in overfitting. The Avramov-Milchev-based model was found to best represent the Hanford low-activity waste glass melt viscosity data based on model fit and validation statistics. A 21-term partial quadratic mixture model was recommended for use. This model predicts melt viscosity with a root-mean square error of $.1736 \ln(P)$, which is similar to the error in viscosity measurements from replicate glass analyses of $.1383 \ln(P)$. Viscosity was found to be most increased by $\text{SiO}_2 > \text{Al}_2\text{O}_3 > \text{ZrO}_2 > \text{SnO}_2$ and most decreased by $\text{Li}_2\text{O} > \text{Na}_2\text{O} > \text{B}_2\text{O}_3 > \text{CaO} > \text{K}_2\text{O} > \text{MgO}$, at temperatures from 900 to 1260°C.

KEYWORDS

borosilicate, composition effects, glass forming melts, glass forming systems, viscosity

1 | INTRODUCTION

Viscosity is a key melt property for glass manufacturing, including nuclear waste vitrification.^{1–5} The optimum viscosity for the Joule-heated ceramic waste glass melters ranges from 20 to 80 Poise (P) at the nominal operating temperature of 1150°C.⁶ A viscosity higher than the optimum range tends to reduce the melter throughput rate

and may cause difficulties in canister filling. Lower viscosities increase corrosion of melt contact materials (refractories, electrodes, bubblers, thermowells, pour-spout trough, etc.) and increase volatility. At Hanford, the nuclear waste glass composition is controlled using glass property-composition models.^{5,7} Lu et al. found that glass compositions designed for optimal immobilization of Hanford low-activity waste (LAW) were nearly all limited by an upper or

This is an open access article under the terms of the [Creative Commons Attribution](https://creativecommons.org/licenses/by/4.0/) License, which permits use, distribution and reproduction in any medium, provided the original work is properly cited.

© 2022 Battelle Memorial Institute. *International Journal of Applied Glass Science* published by American Ceramics Society and Wiley Periodicals LLC. This article has been contributed to by U.S. Government employees and their work is in the public domain in the USA.

TABLE 1 Some of the most frequently referenced viscosity-temperature models in nuclear waste glass science. The table is not intended to be all-inclusive

| Model | Examples | Functions | Pros | Cons |
|--|-------------|--|--|--|
| Arrhenius (AR) | 3,14–17 | $\ln(\eta) = A + \frac{B}{T}$ | <ul style="list-style-type: none"> Fewer parameters Linear fit | <ul style="list-style-type: none"> Only applicable over narrow range |
| Vogel, Fulcher, and Tammann (VF) | 18–25 | $\ln(\eta) = A + \frac{B}{T-T_0}$ | <ul style="list-style-type: none"> Reproduces curvature in data Most widely used in literature | <ul style="list-style-type: none"> Requires nonlinear fit |
| Mauro, Yue, Ellison, Gupta, and Allan (MY) | 10 | $\ln(\eta) = A + \frac{B}{T} \exp\left(\frac{C}{T}\right)$ | <ul style="list-style-type: none"> Reproduces curvature in data Represents data well near glass transition | <ul style="list-style-type: none"> Nonlinear fit |
| Avramov and Milchev (AM) | 10,11,26,27 | $\ln(\eta) = A + \left(\frac{B}{T}\right)^a$ | <ul style="list-style-type: none"> Reproduces curvature in data | <ul style="list-style-type: none"> Nonlinear fit Oddly scaled parameters |

lower viscosity constraint.⁸ Effective models for Hanford waste glass melts are therefore useful and necessary.

Considerable effort has been devoted to the development of models describing silicate melt viscosities as functions of temperature and composition. Reviews and in-depth assessments of modeling approaches and technical underpinnings are readily found in the literature.^{2,9–13} Table 1 presents the most frequently referenced viscosity-temperature models used in the nuclear waste glass industry. Each of the temperature-independent parameters (A , B , T_0 , C , and a) can be expressed as functions of melt composition. To develop effective viscosity models as functions of temperature and composition, a reliable set of data in the desired composition region is needed.

1.1 | Hanford LAW glass property-composition database

A database of glass/melt property-composition data has been collected from 40 separate government reports for the purposes of developing and validating models for operation of the LAW Facility at the Hanford Waste Treatment and Immobilization Plant.²⁸ The database compiles data for 1100 glasses fabricated and tested from 2002 to 2020 by the Catholic University of America (CUA) and the Pacific Northwest National Laboratory (PNNL). All data were collected under the strict nuclear quality assurance (NQA-1) standard.²⁹ The glasses cover the range of compositions currently expected for processing of Hanford LAW in glass (see Table 2) and were formulated using two approaches:

1. Actively designed glasses were formulated to immobilize a specific waste composition while satisfying a

host of property requirements. These glasses, primarily tested by CUA, are most useful for determining the compositions and properties of glasses likely to be processed for a specific waste and tend to have significant correlations in their component concentrations.

2. Statistically designed glasses were formulated to evenly cover a composition space systematically. These glasses, primarily tested by PNNL, tend to minimize correlations between glass component concentrations and are most useful for evaluating composition effects on glass properties.

The glasses were analyzed for viscosity (574), electrical conductivity (567), product consistency test response (796),³⁰ vapor hydration test response (773),³¹ sulfate solubility (626),^{32–34} and Monofrax K-3 refractory neck corrosion (344).³⁵ However, not all properties were measured on each glass composition (numbers in parenthesis represent number of glasses measured for that property). This database of 1100 glasses contains 170 replicate glass compositions, many of which were tested at both CUA and PNNL to allow for the evaluation of property measurement uncertainties.

The viscosities of 574 glasses were measured over the temperature range of 900–1260°C using the rotating spindle method.³⁶ The viscosity data were collected using either a Brookfield viscometer (AMETEK Brookfield, Middleboro, MA) or an Anton Parr viscometer (FRS 1600 Furnace Rheometer System, Ashland, VA). The viscometers (head, Pt crucible, and spindle) were calibrated at room temperature with National Institute of Standards and Technology (NIST) traceable oils and validated at high temperature with standard glasses (NIST standard reference glass 711 or DWPF Startup frit²⁴). A total of 3935 viscosity-temperature datapoints were measured with viscosity values ranging from 2.53 to 7260 P. The

TABLE 2 Hanford low-activity waste (LAW) database glass component concentration ranges (mass fraction)

| Component | Minimum | Maximum | Component | Minimum | Maximum |
|--------------------------------|---------|---------|---|---------|---------|
| Al ₂ O ₃ | .0350 | 0.1475 | P ₂ O ₅ | 0.0000 | 0.0403 |
| B ₂ O ₃ | .0600 | 0.1383 | SO ₃ | 0.0000 | 0.0163 |
| CaO | .0000 | 0.1278 | SiO ₂ | 0.3352 | 0.5226 |
| Cl | .0000 | 0.0117 | SnO ₂ | 0.0000 | 0.0503 |
| Cr ₂ O ₃ | .0000 | 0.0063 | TiO ₂ | 0.0000 | 0.0501 |
| F | .0000 | 0.0130 | V ₂ O ₅ | 0.0000 | 0.0409 |
| Fe ₂ O ₃ | .0000 | .1198 | ZnO | .0000 | .0582 |
| K ₂ O | .0000 | .0590 | ZrO ₂ | .0000 | .0675 |
| Li ₂ O | .0000 | .0584 | SOM [‡] | .0000 | .0033 |
| MgO | .0000 | .0502 | NAlk [*] | .1350 | .2702 |
| Na ₂ O | .0247 | .2657 | SiO ₂ + 1.697Al ₂ O ₃ [§] | .0000 | .6160 |

^{*}NAlk = Na₂O + .66K₂O + 2.07 Li₂O.

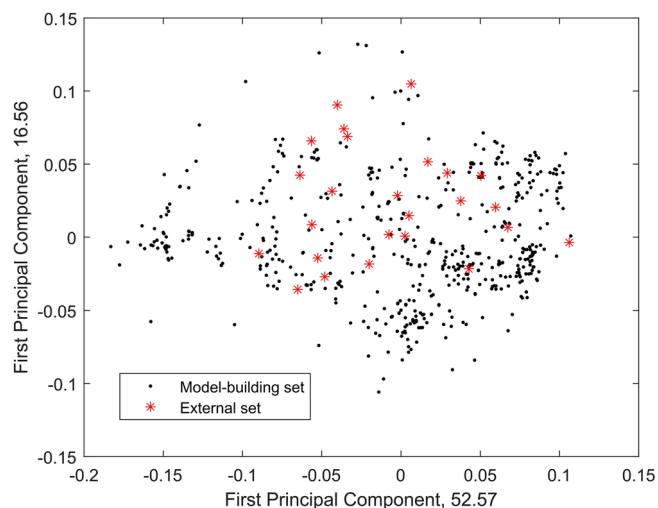
[‡]SOM = sum of minors, including: Ag₂O, BaO, Br, CdO, Cs₂O, I, MnO, MoO₃, NiO, PbO, Re₂O₇, SeO₂, SrO, and WO₃.

[§]A combined SiO₂ and Al₂O₃ constraint was added to avoid region with little data where both these components are high in concentration.

relatively narrow temperature-viscosity ranges were selected to include those immediately adjacent to the planned operating temperature of 1150°C and viscosity range of 20–80 P. In this temperature range, Hanford LAW glasses show Newtonian behavior and are not subject to crystallization, making viscosity determination straightforward. For many of the glasses, the viscosity was measured first at the nominal melting temperature (1150°C) then dropping to the lowest temperature, returning to 1150°C, raising to the maximum temperature, and again returning to 1150°C. This process allowed for the potential effects of crystallization and/or volatility to be assessed.

Evaluation of the compositions of the 574 glasses identified 15 composition outliers (those glasses not falling in the composition region listed in Table 2), which were removed from further evaluation. A dataset containing 25 statistically designed glasses was separated from the database for use as an external model validation set,³⁷ leaving 534 model development glasses with 3765 η -T datapoints. To visualize the space covered by the compositions of the available glasses and assess the coverage of the validation set, a principal component analysis was applied to the composition data. Figure 1 shows a plot of the composition for all 534 model fit composition + 25 external validation compositions using the first two principal components, which accounted for nearly 70% of the total variability in the joint dataset. The plot indicates that glasses in the external validation set provided a good coverage of the overall space, forming a good basis to assess model performance and help in model selection.

The relative standard deviation from replicate glass measurements is on the order of .1383 (based on $\ln(\eta, P)$), suggesting that predictive models will not be able to predict viscosity with higher precision.

**FIGURE 1** Principal components plot of model fit (black dots) and external validation (red asterisks) glass compositions

1.2 | Modeling methodology

Empirical models were developed to predict viscosity (η or resistance to flow) of Hanford LAW glasses as functions of both melt temperature and composition. In this work, the 3765 η -T data were fitted to Arrhenius (AR), Vogel-Fulcher-Tammann (VF), Avramov-Milchev (AM), and Mauro-Yue-Ellison-Gupta-Allen (MY) models, assuming composition dependence of the different temperature-independent parameters (e.g., $A(\mathbf{g})$, $B(\mathbf{g})$, $C(\mathbf{g})$, $T_0(\mathbf{g})$, and $a(\mathbf{g})$). A set of example model forms fitted to the data are shown in Table 3, where \mathbf{g} is the glass composition in mass fractions expressed as a vector; T is the absolute temperature (in K); and A, B, C, T_0 , and a are model parameters that were estimated from the experimental data.

TABLE 3 Model forms used to fit viscosity as a function of glass composition and temperature*

| Type | Single-composition term | Two-composition terms | Three-composition terms |
|------|---|--|--|
| AR | $\ln(\eta) = A(\mathbf{g}) + \frac{B}{T}$ $\ln(\eta) = A + \frac{B(\mathbf{g})}{T}$ | $\ln(\eta) = A(\mathbf{g}) + \frac{B(\mathbf{g})}{T}$ | Not applicable |
| VF | $\ln(\eta) = A(\mathbf{g}) + \frac{B}{(T-T_0)}$ $\ln(\eta) = A + \frac{B(\mathbf{g})}{(T-T_0)}$ $\ln(\eta) = A + \frac{B}{(T-T_0(\mathbf{g}))}$ | $\ln(\eta) = A + \frac{B(\mathbf{g})}{(T-T_0(\mathbf{g}))}$ | $\ln(\eta) = A(\mathbf{g}) + \frac{B(\mathbf{g})}{(T-T_0(\mathbf{g}))}$ |
| AM | $\ln(\eta) = A(\mathbf{g}) + \left(\frac{B}{T}\right)^{\alpha}$ $\ln(\eta) = A + \left(\frac{B(\mathbf{g})}{T}\right)^{\alpha}$ $\ln(\eta) = A + \left(\frac{B}{T}\right)^{\alpha(\mathbf{g})}$ | $\ln(\eta) = A + \left(\frac{B(\mathbf{g})}{T}\right)^{\alpha(\mathbf{g})}$ $\ln(\eta) = A(\mathbf{g}) + \left(\frac{B(\mathbf{g})}{T}\right)^{\alpha}$ | $\ln(\eta) = A(\mathbf{g}) + \left(\frac{B(\mathbf{g})}{T}\right)^{\alpha(\mathbf{g})}$ |
| MY | $\ln(\eta) = A + \frac{B(\mathbf{g})}{T} \exp\left(\frac{C}{T}\right)$ | $\ln(\eta) = A + \frac{B(\mathbf{g})}{T} \exp\left(\frac{C(\mathbf{g})}{T}\right)$ | $\ln(\eta) = A(\mathbf{g}) + \frac{B(\mathbf{g})}{T} \exp\left(\frac{C(\mathbf{g})}{T}\right)$ |

Abbreviations: AM, Avramov-Milchev; AR, Arrhenius; MY, Mauro-Yue-Ellison-Gupta-Allen; VF, Vogel-Fulcher-Tammann.

*An AR-based model was also fitted to a version same dataset with the viscosity values >1000 P removed to improve linearity by Ferkl et al. (2022)³⁹.

Each of these parameters has physical interpretation. For example:

- A is the preexponential or the limiting $\ln(\eta)$ at infinite temperature;
- B is related to the apparent activation energy (by the negative of the universal gas constant);
- C is related to the energy difference between connected and disconnected states; and
- T_0 is the temperature at which $\ln(\eta)$ approaches infinity.

Each parameter in this study was fit to glass compositions using all glass components and a reduced set of glass components by combining those components having little effect on viscosity in the concentration ranges of our database, such as Cl, Cr₂O₃, F, and SO₃, along with sum of minors, into an “Others” term. In general, the modeling approach used to obtain parameter estimates consisted of imputing formatted data in MATLAB (version R2019b, MathWorks, Natick, MA). For AR-based models, ordinary least squares can be directly used to obtain model parameter estimates that are guaranteed to have minimum variance in the class of unbiased linear estimators.³⁸ Nonlinear models were fit using numeric optimization routines `nlinfit` function in MATLAB or Nonlinear Fit in JMP-Pro version 16.0.0 (SAS Institute, Cary, NC). These routines require an initial estimate for the model parameters (seed values), and the result obtained can depend on the input provided to the algorithm. To minimize instability, initial estimates were equal to linear fit values of the similar linear models (e.g., AR), with initial estimates for additional parameters obtained after using the `fminsearch` routine in MATLAB. To ensure stability, model parameter estimates for nonlinear models obtained after using the `nlinfit` function were used as inputs again until no appreciable changes between successive iterations were observed. The MATLAB `nlinfit` function was used for fit-

ting all models. Selected models were checked using the nonlinear fit function in JMP.

Our previous viscosity-temperature-composition modeling effort employed a generalized least squares with split-plot data structure in which the whole-plot was represented by composition and the split-plot by temperature.²⁷ In theory, the split-plot approach makes sense given the structure of the data; however, it is possible that the following assumptions are not applicable to the current dataset: (1) That a constant variance is common to every whole-plot (each composition) and (2) that the variability in terms of the model can be best explained by the whole-plot and split-plot structure. Given that the glasses were fabricated and tested by many people, different laboratories, and over an extended period, it may not be reasonable to assume that the whole-plot variance will remain constant. Application of the whole-plot/split-plot approach to available data resulted in significantly higher prediction error, and larger residuals then were found for ordinary least squares regression and nonlinear regression. For these reasons, the split-plot data structure was not used.

Models were evaluated based on R², adjusted-R² (adj-R²), root-mean-squared errors (RMSEs) for predictions made on the external set of 25 glasses, width of a 90% confidence interval (CI) for a reference glass at 1150°C, and by model complexity. It is well known that when fitting the types of models used in this work, certain interactions between components can have a significant effect on viscosity.⁴⁰ Consideration of higher order terms, like interactions and quadratic effects, can substantially increase the number of potential models that need to be examined, making the analysis of all possible models impractical. Model selection techniques such as forward and backward selection, available in many commercial software packages (e.g., JMP, R, MATLAB), allow for sequential model-building, avoiding the need to explore

all possible models. Stepwise model building algorithms, like forward and backward selection, seek to improve an optimality criterion, such as maximizing R^2 or improving the value of sum-of-squared errors (SSE), by adding or removing the term that most improves the optimality criterion based on the current model until no further improvement is possible. Because these algorithms operate in a locally optimal way, there is no guarantee that a globally optimum model will be found. Additionally, stepwise model selection techniques are not generally available for nonlinear models, further complicating the selection process. For these reasons, only a few models with good performance were selected for additional analysis in most cases.

Additional exploration involved incorporating interactions between pairs of components and quadratic component effects that may produce changes in model predictions that cannot be captured using purely linear component effects. So, the top performing model (AM) was selected to evaluate nonlinear composition terms. This model form has good performance across the measures selected for evaluation and also has among the fewest model parameters. Selecting parsimonious models is generally considered good practice to avoid potential overfitting. In addition to limiting the number of model forms chosen for further analysis, only those components that are likely to have significant interaction effects on viscosity based on previously known results were chosen for additional model development. Components selected for inclusion as higher order terms are Al_2O_3 , B_2O_3 , K_2O , Li_2O , Na_2O , CaO , SiO_2 , and ZrO_2 . All possible combinations of one purely quadratic term and one, two, and three two-factor interactions of these components were considered. This resulted in 1142 AM partial quadratic models (PQMs) fitted for evaluation.

As with the initial analysis of all model forms, goodness of fit statistics, including RMSE, R^2 , and adj- R^2 for the modeling set and prediction $\text{SSE}(= \sum[\ln(\eta)_{\text{pred}} - \ln(\eta)_{\text{meas}}]^2)$ (or validation RMSE) using data from the 25-glass external validation set, were used to evaluate model performance. These results guided the selection of one or more models to be used in practice. The width of a 90% CI for $\ln(\eta)$ prediction at 1150°C for a representative glass composition was also used as a parameter for evaluating model quality.³⁸

2 | RESULTS

The 17 models described in Table 3 were fitted to 3765 η -T data, and the resulting models were used to predict the response of the 25-glass (150 η -T data point) external validation set. It was apparent from the fits that all AR-

based models resulted in curvature in the residuals versus predicted plot (as shown in Figure 2A). This curvature was present in both the AR models and the MY single-composition-term model and not in any of the other models. For comparison, Figure 2B shows the residuals versus predicted plot for the single-composition-term VF models, which is typical of all other models. The bias predictions observed with the AR model are due to the inherent curvature in $\ln(\eta)$ versus inverse temperature in fragile liquids¹⁰ that can be seen even over the narrow viscosity range of this data (2.53–7260 P or .9–9 $\ln(P)$). The statistics of each of the fits are summarized in Table 4.

Figure 3 shows the R^2 values from model fit, subset validation, 25-glass external validation set, and 90% CI average width for the glasses in the modeling set as functions of the number of model terms and model type. For each model form, if only one term is composition-dependent, the B -term yields the best results (followed by A for AR form, T_0 for VF form, and a for AM form).

The model fit and subset validation statistics improve with the number of terms for each model form nearly across the board. The exception to this trend is the single composition term models with non- B composition terms. The trend is different for the 25-glass external validation statistics, where often models with the most terms produce worse results than simpler, smaller ones, potentially indicating overfitting. The average 90% CI width generally grows with the number of parameters with AR-based models being higher. Although the ranking of models differed between evaluation statistics, the AM models were generally ranked the best for each evaluation statistic. Of the AM models, the single-composition-term reduced-linear-mixture (RLM) performed best on the validation set R^2 among models with the fewest terms. Therefore, the AM 1B-RLM model, the model with B as the only composition-dependent term, was selected for further analysis. The coefficients for the models developed using the AM 1B-RLM as a starting point are listed in Table 5, and predicted versus measured plot is given in Figure 4. The coefficients and summary statistics for the best fitting AR, VF, and MY models are given in *Supplemental Information Table S1*.

Plots of SSEs for prediction on the 25-glass external validation set against the RMSE for modeling set using the AM PQMs are shown in Figure 5. Figure 6 shows the widths of 90% CIs for a reference glass (roughly center of composition region) against the adj- R^2 for the 1142 PQMs models. There is a broad range of goodness parameters across the 1142 PQMs with different rankings of models depending on which parameter is selected. (Shorter CIs are generally associated with better predictive performance.)³⁸ The model with the following cross-product and quadratic terms was selected based on the lowest validation set SSE

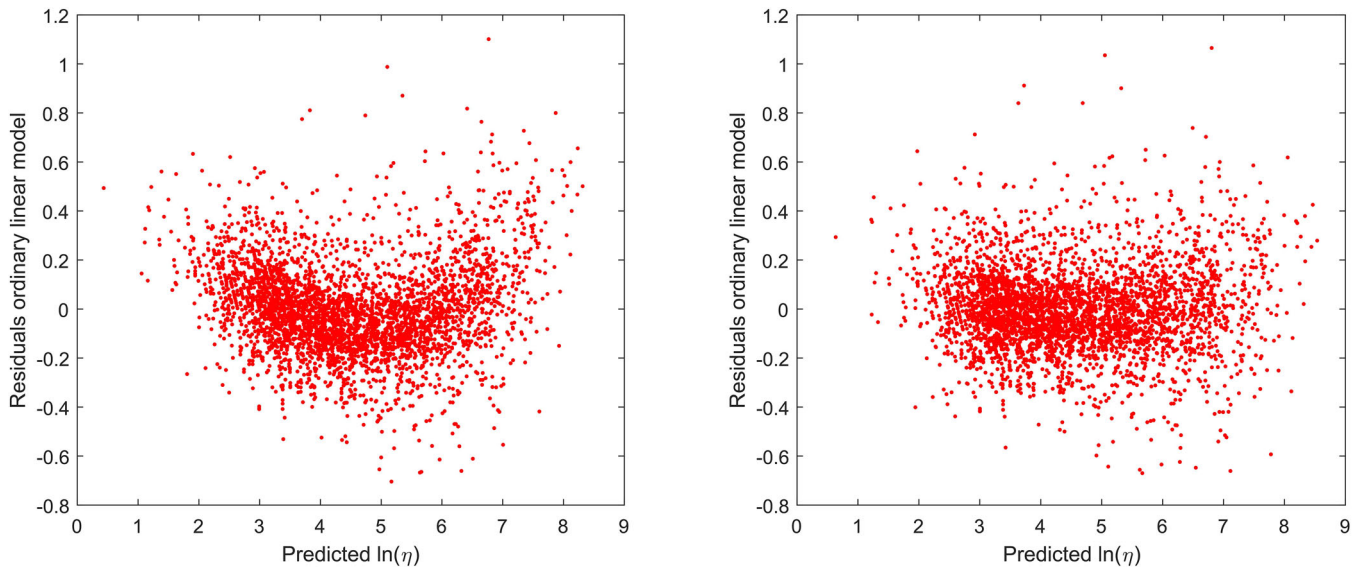


FIGURE 2 Example residual versus predicted plots (where $\ln(\eta)$ is shown in $\ln(P)$) for (A) AR and (B) VF single-composition-term models

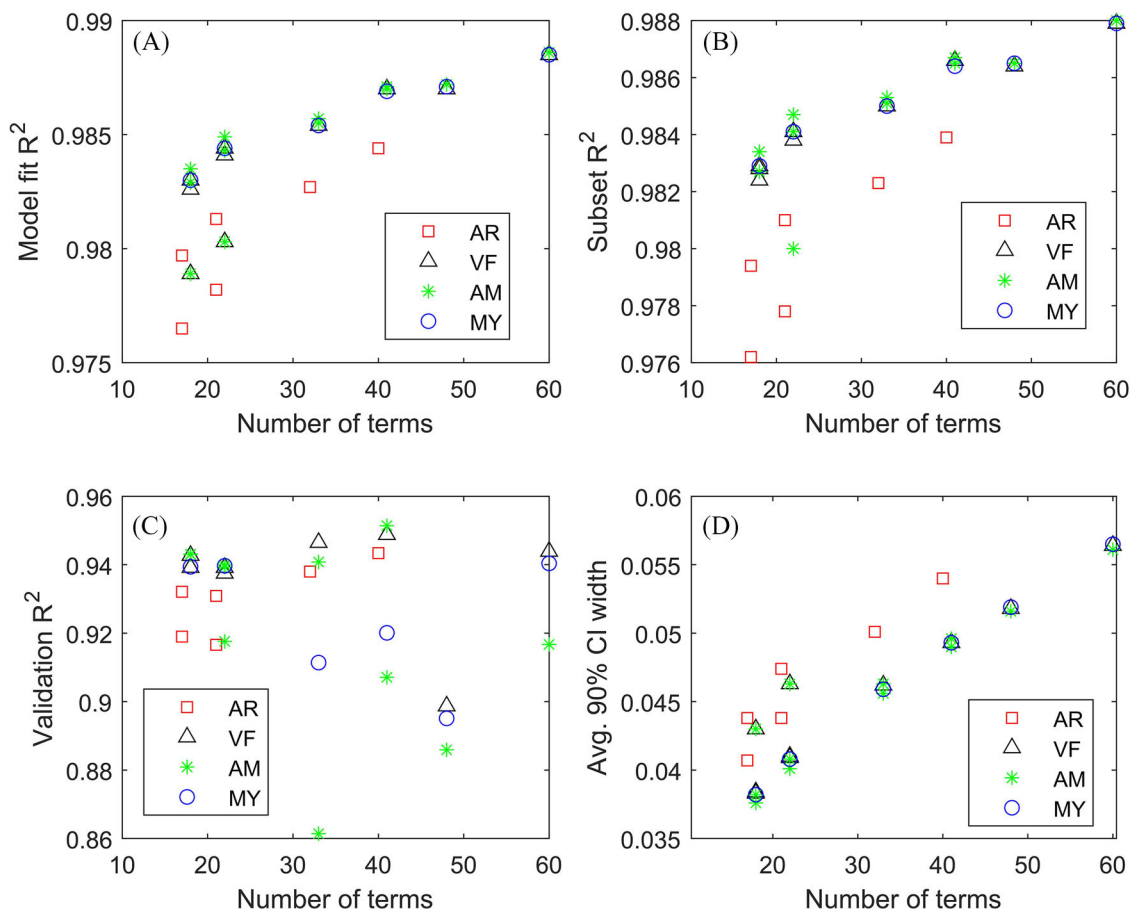


FIGURE 3 R^2 values for model fit as a function of number of model terms for (A) model fit, (B) subset validation, (C) 25-glass external validation, and (D) average width of the 90% confidence intervals for the modeling dataset

TABLE 4 Summary of model fit and validation statistics

| Model | g Form | # of parameters | Fit RMSE | Fit R ² | Fit Adj-R ² | Subset RMSE | Subset R ² | Val RMSE | Val R ² | Average 90% CI width |
|-------|--------|-----------------|----------|--------------------|------------------------|-------------|-----------------------|----------|--------------------|----------------------|
| AR | 1A-FLM | 21 | .204 | .9782 | .9781 | .206 | .9778 | .236 | .9166 | .0474 |
| | 1A-RLM | 17 | .212 | .9765 | .9764 | .213 | .9762 | .232 | .9190 | .0438 |
| | 1B-FLM | 21 | .189 | .9813 | .9812 | .190 | .9810 | .215 | .9309 | .0438 |
| | 1B-RLM | 17 | .197 | .9797 | .9796 | .198 | .9794 | .213 | .9321 | .0407 |
| | 2-FLM | 40 | .173 | .9844 | .9842 | .175 | .9839 | .194 | .9434 | .0540 |
| | 2-RLM | 32 | .182 | .9827 | .9826 | .184 | .9823 | .203 | .9380 | .0501 |
| VF | 1A-FLM | 22 | .194 | .9803 | .9802 | .174 | .9841 | .201 | .9392 | .0463 |
| | 1A-RLM | 18 | .201 | .9789 | .9788 | .181 | .9828 | .201 | .9392 | .0430 |
| | 1B-FLM | 22 | .173 | .9844 | .9843 | .174 | .9841 | .201 | .9392 | .0409 |
| | 1B-RLM | 18 | .180 | .9830 | .9829 | .181 | .9829 | .201 | .9392 | .0383 |
| | 1T-FLM | 22 | .175 | .9841 | .9840 | .176 | .9838 | .204 | .9375 | .0410 |
| | 1T-RLM | 18 | .182 | .9826 | .9825 | .183 | .9824 | .195 | .9427 | .0384 |
| | 2-FLM | 41 | .158 | .9870 | .9869 | .160 | .9866 | .185 | .9488 | .0493 |
| | 2-RLM | 33 | .167 | .9854 | .9853 | .169 | .9850 | .189 | .9465 | .0462 |
| | 3-FLM | 60 | .150 | .9885 | .9883 | .152 | .9879 | .193 | .9439 | .0564 |
| 3-RLM | 48 | .158 | .9870 | .9869 | .161 | .9864 | .260 | .8987 | .0518 | |
| AM | 1A-FLM | 22 | .194 | .9803 | .9802 | .195 | .9800 | .234 | .9176 | .0463 |
| | 1A-RLM | 18 | .201 | .9789 | .9788 | .178 | .9834 | .195 | .9431 | .0430 |
| | 1B-FLM | 22 | .170 | .9849 | .9848 | .171 | .9847 | .200 | .9400 | .0401 |
| | 1B-RLM | 18 | .178 | .9835 | .9835 | .178 | .9834 | .195 | .9431 | .0376 |
| | 1a-FLM | 22 | .173 | .9843 | .9842 | .174 | .9841 | .201 | .9393 | .0408 |
| | 1a-RLM | 18 | .181 | .9829 | .9828 | .182 | .9827 | .195 | .9430 | .0382 |
| | 2a-FLM | 41 | .158 | .9870 | .9869 | .160 | .9865 | .249 | .9071 | .0490 |
| | 2a-RLM | 33 | .167 | .9855 | .9854 | .169 | .9851 | .304 | .8614 | .0456 |
| | 2A-FLM | 41 | .158 | .9871 | .9870 | .159 | .9867 | .180 | .9514 | .0496 |
| | 2A-RLM | 33 | .166 | .9857 | .9855 | .168 | .9853 | .199 | .9408 | .0463 |
| 3-FLM | 60 | .149 | .9886 | .9884 | .151 | .9880 | .236 | .9167 | .0561 | |
| 3-RLM | 48 | .157 | .9872 | .9871 | .160 | .9865 | .276 | .8859 | .0516 | |
| MY | 1-FLM | 22 | .173 | .9844 | .9843 | .174 | .9841 | .200 | .9397 | .0408 |
| | 1-RLM | 18 | .180 | .9830 | .9829 | .181 | .9829 | .201 | .9394 | .0382 |
| | 2-FLM | 41 | .159 | .9869 | .9868 | .161 | .9864 | .231 | .9201 | .0493 |
| | 2-RLM | 33 | .168 | .9854 | .9853 | .169 | .9850 | .243 | .9114 | .0459 |
| | 3-FLM | 60 | .150 | .9885 | .9883 | .152 | .9879 | .199 | .9404 | .0565 |
| | d3-RLM | 48 | .158 | .9871 | .9870 | .160 | .9865 | .265 | .8951 | .0519 |

Abbreviations: AM, Avramov-Milchev; AR, Arrhenius; CI, confidence interval; MY, Mauro-Yue-Ellison-Gupta-Allen; FLM, full-linear-mixture; RLM, reduced-linear-mixture; RMSE, root mean squared errors; VF, Vogel-Fulcher-Tammann.

and generally low model fit RMSE and 90% CI width: $\text{Al}_2\text{O}_3 \times \text{Na}_2\text{O}$, $\text{SiO}_2 \times \text{ZrO}_2$, and $\text{Na}_2\text{O} \times \text{Na}_2\text{O}$. Note that no single model performed best on all criteria.

Table 5 lists model parameter estimates for the selected model. A plot of predicted versus measured $\ln(\eta)$ is given in Figure 7. Model fit and external validation statistics were significantly improved by the addition of three non-linear terms.

3 | DISCUSSION

There is a need for accurate and precise prediction of Hanford LAW glass melt viscosity to optimize glass composition and facilitate efficient plant operations. By evaluating a series of example temperature-composition-viscosity models, it became clear that there are multiple potentially successful models all with RMSEs on the same order as

TABLE 5 Selected single-composition-term RLM and PQM model coefficients for the AM model form*

| Term | AM RLM | AM PQM |
|--|------------|------------|
| A | -2.0579 | -2.1483 |
| A | 2.2838 | 2.2520 |
| Al ₂ O ₃ | 5701.7808 | 4522.3515 |
| B ₂ O ₃ | 942.3703 | 1020.4357 |
| CaO | 1106.2752 | 1260.0231 |
| Fe ₂ O ₃ | 2599.7249 | 2762.4187 |
| K ₂ O | 1444.3510 | 1673.1286 |
| Li ₂ O | -5365.8759 | -5264.2734 |
| MgO | 2182.2295 | 2373.9846 |
| Na ₂ O | 409.3835 | 291.4697 |
| P ₂ O ₅ | 3636.8594 | 3984.1403 |
| SiO ₂ | 4793.7353 | 4921.0864 |
| SnO ₂ | 4140.2617 | 4388.7692 |
| TiO ₂ | 2260.8158 | 2401.3011 |
| V ₂ O ₅ | 1766.1165 | 1985.4762 |
| ZnO | 1768.2457 | 1826.5884 |
| ZrO ₂ | 4581.3414 | 3659.8543 |
| Others | 3572.0333 | 3503.1550 |
| Al ₂ O ₃ × Na ₂ O | n/a | 7674.5414 |
| SiO ₂ × ZrO ₂ | n/a | 2602.8079 |
| Na ₂ O × Na ₂ O | n/a | -996.9091 |
| Fit R ² | .9835 | .9843 |
| Fit RMSE | .1775 | .1736 |
| Val R ² | .9701 | .9755 |
| Val RMSE | .1947 | .1762 |

Abbreviations: AM, Avramov-Milchev; PQM partial quadratic model; RLM, reduced-linear-mixture; RMSE, root mean squared errors, n/a, not applicable.

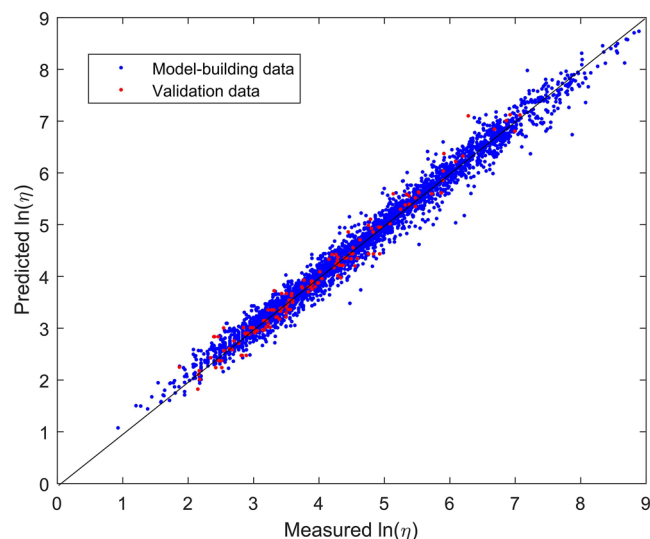


FIGURE 4 Predicted versus measured $\ln(\eta, P)$ for the single-composition-term reduced-linear-mixture (RLM) Avramov-Milchev (AM) model. Blue points represent points used during model-building, and red points represent validation points

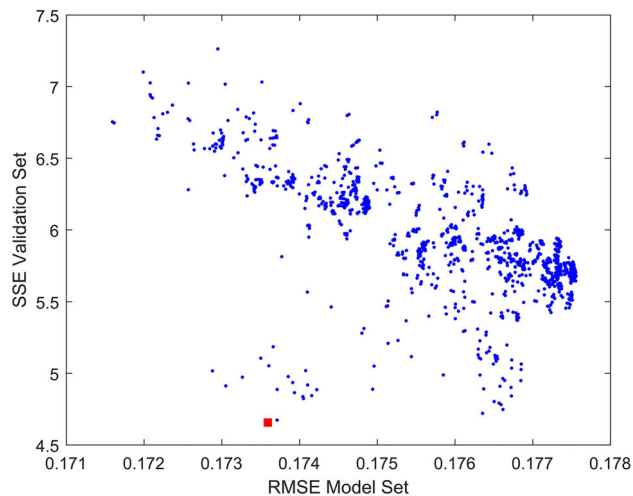


FIGURE 5 Sum-of-Squared Errors (SSE) for predictions using the 25-glass external validation set against the root-mean-squared errors (RMSEs) (in $\ln(P)$) for the modeling set for each of the 1142 partial quadratic model (PQM) models. Red square is the recommended model

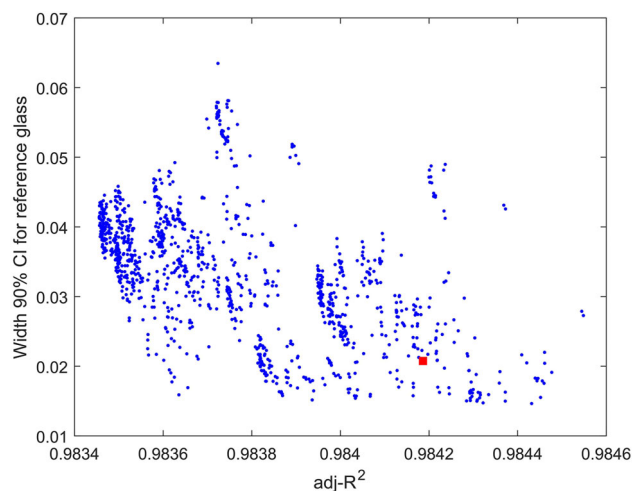


FIGURE 6 Widths of 90% confidence intervals (CIs) (in $\ln(P)$) for a reference glass at 1150°C against the adj-R^2 for modeling set for 1142 partial quadratic model (PQM) models. Red square is the recommended model

the experimental uncertainty obtained from replicate glass measurement (.138 $\ln(P)$). Even so, the AM model form does seem to slightly outperform the other tested forms for this dataset.

It was interesting to see that for model forms AR, VF, and AM, which fit one of the temperature-independent values as a function of composition (\mathbf{g}), the goodness of fit was similar no matter which temperature-independent parameter was composition dependent (a, A, B, T_0). However, in each case, there was a slight advantage of fitting $B(\mathbf{g})$ over the other parameters. This suggests that the most

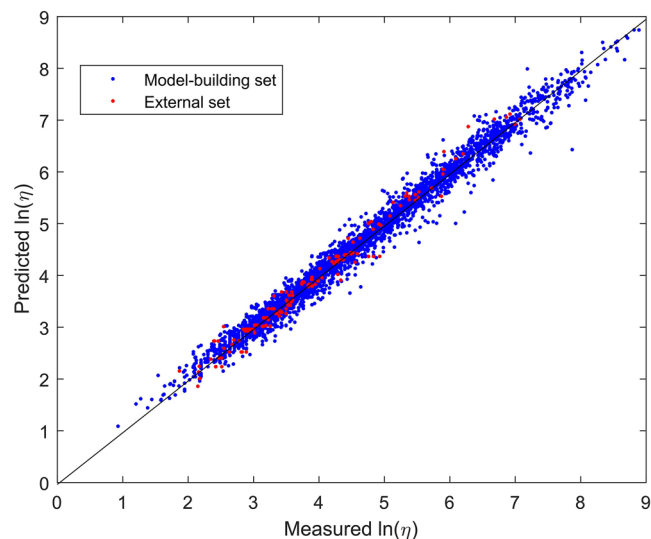


FIGURE 7 Predicted versus measured $\ln(\eta, P)$ for the selected partial quadratic model (PQM) model. Blue points represent model fit data; red points represent validation data

significant compositional effect in this composition region is related to the apparent activation energy for viscous flow. Fitting multiple parameters as functions of composition tended to reduce the model fit RMSE but increased the validation RMSE, suggesting an overfitting.

The AR-based models showed biased predictions with a clear curvature pattern present in the residual plot due to the general fragility of these melts; Figure S1 in the *Supplemental Information* compares the fragility of a representative subset of these melts with the liquids evaluated by Angell.⁴¹ The AM model does not represent the full temperature-viscosity relationship, nor do any models fitted to such a narrow range of viscosity values. To demonstrate that point, the best fitting AR, AM, VF, and MY models (from *Supplemental Information* Section S3) are used to predict the response of one of the dataset glasses and extrapolated to high- and low-temperatures in Figure 8. The glass, LAWA44, was selected for this demonstration because it was measured in replicate and had replicate glass transition temperature (T_g) measurements. T_g is plotted on the figure with an assumed viscosity of 10^{13} P. It is interesting that three of the four models result in reasonable correlation to the assumed $\log[\eta_{T_g}, P] = 13$ with the VF nearly predicting the value exactly. However, the AM model should not be extrapolated down in temperature. The three nonlinear models (AM, VF, and MY) all predict similar infinite temperature viscosities: $10^{-1.93}$, $10^{-2.71}$, and $10^{-2.41}$ Pa·s, respectively – close to but above the universal infinite temperature viscosity identified by Zheng for silicate liquids ($10^{-2.93}$ Pa·s).⁴² To precisely obtain the infinite temperature viscosity for Hanford LAW glasses would

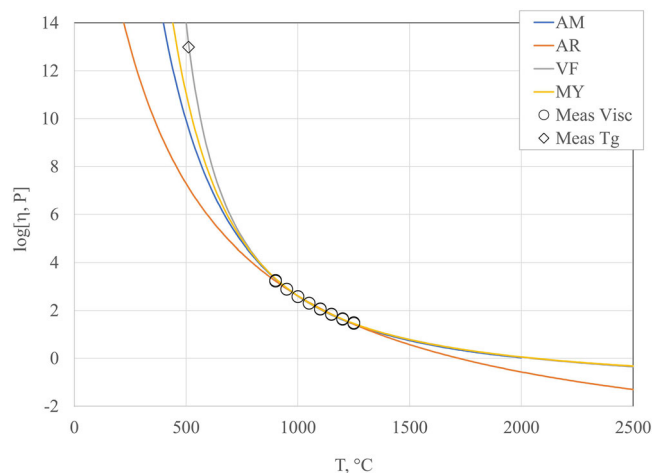


FIGURE 8 Extrapolation of viscosity predictions of LAWA44 glass to high- and low-temperature

require viscosity data over a broader temperature range than was available in this dataset.

The composition effects on viscosity can be estimated using response trace plots (plots showing the effect on the response to increasing or decreasing concentration of a single component for a reference glass while relative proportions of the rest remain constant). Figure 9 shows response trace plots for the selected AM-PQM model at 950, 1050, 1150, and 1250°C taken at the reference glass composition. These plots were generated by selecting a reference composition (the nominal average of compositions in the database) and varying one-component-at-a-time over its available range while renormalizing the other component concentrations. The predicted $\ln(\eta, P)$ values obtained are then plotted versus component concentration change. From the plots, it can be seen that across all temperatures, viscosity is most increased by $\text{SiO}_2 > \text{Al}_2\text{O}_3 > \text{ZrO}_2 > \text{SnO}_2$ and most decreased by $\text{Li}_2\text{O} > \text{Na}_2\text{O} > \text{B}_2\text{O}_3 > \text{CaO} > \text{K}_2\text{O} > \text{MgO}$. Many previous studies have shown similar component effects ranking for viscosity.^{9,14-17,23,43-45} As expected, the effects of alkali group oxides, alkaline earth group oxides, and SiO_2 , Al_2O_3 , ZrO_2 , and SnO_2 are in order with cation field strength.

4 | CONCLUSION

A database suitable for modeling the key properties of Hanford LAW glasses was collected, including viscosity data for 574 glasses with viscosities ranging from 2.53 to 7260 P within the temperature range of 900–1260°C. A total of 3765 of the 3935 η -T-composition datapoints were used to develop viscosity models as functions of both temperature and composition, with an additional 150 points reserved for validation. Nearly 3000 different models were developed

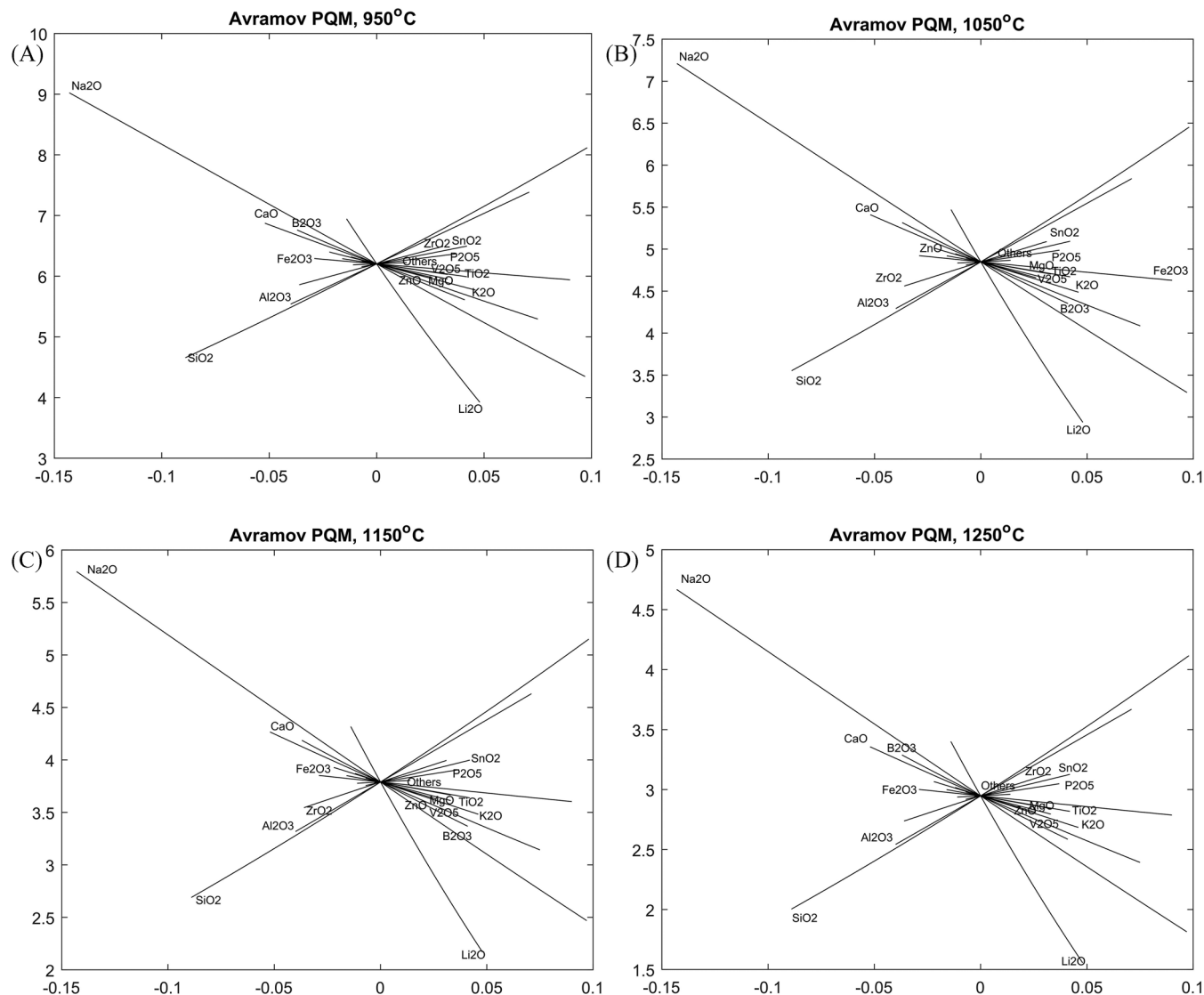


FIGURE 9 Component response trace plots of predicted $\ln(\eta, P)$ versus single component concentration change from reference glass composition (in mass fraction) at various temperatures

based on AR, AM, VF, and MY functional forms with composition represented as full- and reduced-linear-mixture and partial-quadratic-mixture models (FLM, RLM, PQM; respectively). These models were evaluated using standard statistical measures. Many of the models were found to predict $\ln(\eta)$ roughly as precisely as it can be measured (based on results from replicate measurements), although of all the models, those based on the AM appeared to perform the best for this dataset. A 21-parameter PQM based on AM functional form was recommended for use in design of glasses and control of melter operation at the Hanford Site (with a variance-covariance matrix in *Supplemental Information* Section S3). This model accurately predicts $\ln(\eta)$ with a precision (RMSE) of .1736 $\ln(P)$, close to that of replicate glass measurement uncertainty. This model is not appropriate for extrapolation in either temperature or com-

position from the ranges used in its development. Different aspects of model fitting and composition-temperature effects on viscosity are also presented for use by the broader glass science arena.

ACKNOWLEDGMENTS

This research was funded by the U.S. Department of Energy (DOE) Office of River Protection (ORP) under the Waste Treatment Plant Project. The authors are thankful for the support, motivation, and oversight. They are also thankful to Pavel Hrma (AttainX, General Service Support Contractor to ORP) and Greg Piepel (retired PNNL) for helpful conversations and suggestions related to this work. They are indebted to the Catholic University of America (and in particular Prof. Ian Pegg) for sharing of their data, which represents a significant portion of the viscosity

dataset used in this study and two anonymous reviewers whose comments significantly improved this article. Pacific Northwest National Laboratory is operated by Battelle for the DOE under contract DEAC05-76RL01830.

CONFLICT OF INTEREST

The authors declare that there is no conflict of interest.

ORCID

Charmayne E. Lonergan  <https://orcid.org/0000-0003-2667-4815>

Albert A. Kruger  <https://orcid.org/0000-0001-8468-0813>

John D. Vienna  <https://orcid.org/0000-0002-6832-9502>

REFERENCES

- Capps W. Viscosity of glass. *J Colloid Sci.* 1952;7(3):334–42, [https://doi.org/10.1016/0095-8522\(52\)90079-2](https://doi.org/10.1016/0095-8522(52)90079-2).
- Fotheringham U. Viscosity of glass and glass-forming melts. In: Musgraves JD, Hu J, Calvez L, editors. *Springer handbook of glass*. Cham, Switzerland: Springer, Nature; 2019. p. 79–112.
- Hrma P, Arrigoni BM, Schweiger MJ. Viscosity of many-component glasses. *J Non-Cryst Solids.* 2009;355(14–5):891–902. <https://doi.org/10.1016/j.jnoncrysol.2009.03.005>.
- Kim D. Glass property models, constraints, and formulation approaches for vitrification of high-level nuclear wastes at the us Hanford site. *J. Korean Ceram. Soc.* 2015;52(2):92, <https://doi.org/10.4191/kcers.2015.52.2.92>.
- Vienna JD. Compositional models of glass/melt properties and their use for glass formulation. *Procedia Mater Sci.* 2014;7:148–55, <https://doi.org/10.1016/j.mspro.2014.10.020>.
- Perez JM. Practical and historical bases for a glass viscosity range for joule-heater ceramic melter operation, CCN: 150054. Richland, WA: River Protection Project, Hanford Tank Waste Treatment and Immobilization Plant; 2006.
- Kim DS, Vienna JD. Preliminary ILAW formulation algorithm description: 24590-LAW-RPT-RT-04-0003, Rev. 1, ORP-56321. Richland, WA: River Protection Project, Hanford Tank Waste Treatment and Immobilization Plant; 2012.
- Lu X, Kim DS, Vienna JD. Impacts of constraints and uncertainties on projected amount of Hanford low-activity waste glasses. *Nucl Eng Des.* 2021;385:111543. <https://doi.org/10.1016/j.nucengdes.2021.111543>.
- Fluegel A. Glass viscosity calculation based on a global statistical modelling approach. *Glass Technol.* 2007;48(1):13–30.
- Mauro JC, Yue YZ, Ellison AJ, Gupta PK, Allan DC. Viscosity of glass-forming liquids. *Proc Nat Acad Sci USA.* 2009;106(47):19780–4, <https://doi.org/10.1073/pnas.0911705106>.
- Ojovan MI. Viscosity and glass transition in amorphous oxides. *Adv Condens Matter Phys.* 2008. <https://doi.org/10.1155/2008/817829>.
- Ojovan M. Viscous flow and the viscosity of melts and glasses. *Phys Chem Glasses, Eur J Glass Sci Technol B.* 2012;53(4):143–50.
- Cassar DR. Viscnet: neural network for predicting the fragility index and the temperature-dependency of viscosity. *Acta Mater.* 2021;206:116602, <https://doi.org/10.1016/j.actamat.2020.116602>.
- Hrma P. Arrhenius model for high-temperature glass-viscosity with a constant pre-exponential factor. *J Non-Cryst Solids.* 2008;354(18):1962–8, <https://doi.org/10.1016/j.jnoncrysol.2007.11.016>.
- Hrma P, Han SS. Effect of glass composition on activation energy of viscosity in glass-melting-temperature range. *J Non-Cryst Solids.* 2012;358(15):1818–29, <https://doi.org/10.1016/j.jnoncrysol.2012.05.030>.
- Hrma P, Kruger AA. High-temperature viscosity of many-component glass melts. *J Non-Cryst Solids.* 2016;437:17–25, <https://doi.org/10.1016/j.jnoncrysol.2016.01.007>.
- Vienna JD, Kim DS, Hrma P. Database and interim glass property models for Hanford HLW and LAW Glasses, PNNL-14060. Richland, WA: Pacific Northwest National Laboratory; 2002.
- Vogel H. Das temperaturabhängigkeitsgesetz der viskosität von flüssigkeiten. *Zeitschrift für Physik.* 1921;22:645–46.
- Tammann G, Hesse W. The dependence of viscosity upon the temperature of supercooled liquids. *Z Anorg Allg Chem.* 1926;156(1):245–57.
- Fulcher GS. Analysis of recent measurements of the viscosity of glasses. II. *J Am Ceram Soc.* 1925;8(12):789–94, <https://doi.org/10.1111/j.1151-2916.1925.tb18582.x>.
- Vienna JD, Kim DS, Skorski DC, Matyas J. Glass property models and constraints for estimating the glass to be produced at hanford by implementing current advanced glass formulation efforts, PNNL-22631. Richland, WA: Pacific Northwest National Laboratory; 2013.
- Jantzen CM. First-principle process product models for vitrification of nuclear waste: relationship of glass composition to glass viscosity, resistivity, liquidus temperature, and durability. *Ceram Trans.* 1991;23:37–51.
- Vienna JD, Hrma P, Kim DS, Schweiger MJ, Smith DE. Compositional dependence of viscosity, electrical conductivity, and liquidus temperature of multicomponent borosilicate waste glasses. *Ceram Trans.* 1996;72:427–36.
- Crum JV, Edwards TB, Russell RL, Workman PJ, Schweiger MJ, Schumacher RF, et al. DWPF startup frit viscosity measurement round robin results. *J Am Ceram Soc.* 2012;95(7):2196–205, <https://doi.org/10.1111/j.1551-2916.2012.05220.x>.
- Hrma P, Piepel GF, Redgate PE, Smith DE, Schweiger MJ, Vienna JD, et al. Prediction of processing properties for nuclear waste glasses. *Ceram Trans.* 1995;61:505–13.
- Avramov I, Milchev A. Effect of disorder on diffusion and viscosity in condensed systems. *J Non-Cryst Solids.* 1988;104(2–3):253–60, [https://doi.org/10.1016/0022-3093\(88\)90396-1](https://doi.org/10.1016/0022-3093(88)90396-1).
- Piepel GF, Heredia-Langner A, Cooley SK. Property-composition-temperature modeling of waste glass melt data subject to a randomization restriction. *J Am Ceram Soc.* 2008;91(10):3222–8, <https://doi.org/10.1111/j.1551-2916.2008.02590.x>.
- Vienna JD, Heredia-Langner A, Cooley SK, Holmes AE, Kim DS, Lumetta NA. Glass property-composition models for support of Hanford WTP LAW facility operation, PNNL-30932. Richland, WA: Pacific Northwest National Laboratory; 2020.
- ASME. Quality assurance requirements for nuclear facility applications, ASME-NQA-1. New York, NY: American Society of Mechanical Engineers; 2008.
- ASTM. Standard test methods for determining chemical durability of nuclear, hazardous, and mixed waste glasses and

- multiphase glass ceramics: the product consistency test (PCT), ASTM C1285-08. West Conshohocken, PA: ASTM International; 2008.
31. ASTM. Standard test method for measuring waste glass or glass ceramic durability by vapor hydration test, ASTM C1663-09. West Conshohocken, PA: ASTM International; 2009.
 32. Jin T, Kim DS, Darnell LP, Weese BL, Canfield NL, Bliss M, et al. A crucible salt saturation method for determining sulfur solubility in glass melt. *Int J Appl Glass Sci.* 2019;10:92–102, <https://doi.org/10.1111/ijag.12366>.
 33. Skidmore CH, Vienna JD, Jin T, Kim DS, Stanfill BA, Fox KM, et al. Sulfur solubility in low activity waste glass and its correlation to melter tolerance. *Int J Appl Glass Sci.* 2019;10(4):558–68, <https://doi.org/10.1111/IJAG.13272>.
 34. Vienna JD, Kim DS, Muller IS, Piepel GF, Kruger AA. Toward understanding the effect of low-activity waste glass composition on sulfur solubility. *J Am Ceram Soc.* 2014;97(10):3135–42, <https://doi.org/10.1111/jace.13125>.
 35. Muller IS, Gilbo K, Chaudhuri M, Pegg IL, Joseph I. K-3 refractory corrosion and sulfate solubility model enhancement, VSL-18R4360-1. Washington, D.C.: Vitreous State Laboratory, the Catholic University of America; 2018.
 36. ASTM. Standard practice for measuring viscosity of glass above the softening point, ASTM C965-12. West Conshohocken, PA: ASTM International; 2012.
 37. Gervasio V, Vienna JD, Lang JB, Westman BE, Sannoh SE, Russell RL, et al. Enhanced Hanford low-activity waste glass property data development: phase 4, PNNL-31556. Richland, WA: Pacific Northwest National Laboratory; 2021.
 38. Myers R, Montgomery D, Vining G. Generalized linear models with applications in engineering and the sciences. Hoboken, NJ: Wiley; 2002.
 39. Ferkl P, Hrma P, Kruger AA. Parsimonious viscosity–composition relationships for high-temperature multicomponent glass melts. *J Asian Ceramic Soc.* 2022. <https://doi.org/10.1080/21870764.2021.2012903>.
 40. Fluegel A. Glass viscosity calculation based on a global statistical modelling approach. *Glass Technol– Eur J Glass Sci Technol Part A.* 2007;48(1):13–30.
 41. Angell CA. Relaxation in liquids, polymers and plastic crystals – strong/fragile patterns and problems. *J Non-Cryst Solids.* 1991;131–3:13–31, [https://doi.org/10.1016/0022-3093\(91\)90266-9](https://doi.org/10.1016/0022-3093(91)90266-9).
 42. Zheng Q, Mauro JC, Ellison AJ, Potuzak M, Yue Y. Universality of the high-temperature viscosity limit of silicate liquids. *Phys Rev B.* 2011;83(21):212201, <https://doi.org/10.1103/PhysRevB.83.212202>.
 43. Vienna JD, Fluegel A, Kim DS, Hrma P. Glass property data and models for estimating high-level waste glass volume, PNNL-18501. Richland, WA: Pacific Northwest National Laboratory; 2009.
 44. Vienna JD, Piepel GF, Kim DS, Crum JV, Lonergan CE, Stanfill BA, et al. 2016 update of Hanford glass property models and constraints for use in estimating the glass mass to be produced at Hanford by implementing current enhanced glass formulation efforts, PNNL-25835. Richland, WA: Pacific Northwest National Laboratory; 2016.
 45. Vienna JD, Heredia-Langner A, Cooley SK, Holmes AE, Kim DS, Lumetta NA. Glass property-composition models for support of Hanford WTP LAW facility operation, PNNL-30932, Rev. 2. Richland, WA: Pacific Northwest National Laboratory; 2022.

SUPPORTING INFORMATION

Additional supporting information may be found in the online version of the article at the publisher's website.

How to cite this article: Heredia-Langner A, Gervasio V, Cooley SK, Lonergan CE, Kim DS, Kruger AA, et al. Hanford low-activity waste glass composition-temperature-melt viscosity relationships. *Int J Appl Glass Sci.* 2022;13:514–525. <https://doi.org/10.1111/ijag.16580>